Geophysical Research Letters

RESEARCH LETTER
10.1029/2023GL106501

Key Points:

- Widespread buoyancy loss across the Irminger interior and Irminger Current (IC) delayed the recovery of the interior from strong cooling in 2015
- Baroclinic instabilities shed from the IC are the dominant source of buoyancy restratifying the sub-surface Irminger interior
- It is important to consider changes in the IC when considering drivers of variability in convection, ventilation, and the Atlantic Meridional Overturning Circulation

Supporting Information:

Supporting Information may be found in the online version of this article.

Correspondence to:

M. Nelson,
m3nelson@ucsd.edu

Citation:

Nelson, M., Straneo, F., Purkey, S. G., & de Jong, M. F. (2024). Delayed recovery of the Irminger interior from cooling in 2015 due to widespread buoyancy loss and suppressed restratification. *Geophysical Research Letters*, *51*, e2023GL106501. https://doi.org/10.1029/2023GL106501

Received 2 OCT 2023
Accepted 6 JAN 2024

Author Contributions:

Conceptualization: Monica Nelson, Fiamma Straneo, Sarah G. Purkey, Marieke Femke de Jong
Data curation: Fiamma Straneo, Marieke Femke de Jong
Formal analysis: Monica Nelson
Funding acquisition: Fiamma Straneo
Investigation: Monica Nelson
Methodology: Monica Nelson, Fiamma Straneo, Sarah G. Purkey
Supervision: Fiamma Straneo, Sarah G. Purkey
Visualization: Monica Nelson

Delayed Recovery of the Irminger Interior From Cooling in 2015 Due To Widespread Buoyancy Loss and Suppressed Restratification

Monica Nelson[1], Fiamma Straneo[1], Sarah G. Purkey[1], and Marieke Femke de Jong[2]

[1]Scripps Institution of Oceanography, University of California San Diego, La Jolla, CA, USA, [2]Department of Ocean Systems, NIOZ, Royal Netherlands Institute for Sea Research, Den Burg, The Netherlands

Abstract Watermass transformation in the Irminger Sea, a key region for the Atlantic Meridional Overturning Circulation, is influenced by atmospheric and oceanic variability. Strong wintertime atmospheric forcing in 2015 resulted in enhanced convection and the densification of the Irminger Sea. Deep convection persisted until 2018, even though winters following 2015 were mild. We show that this behavior can be attributed to an initially slow convergence of buoyancy, followed by more rapid convergence of buoyancy. This two-stage recovery, in turn, is consistent with restratification driven by baroclinic instability of the Irminger Current (IC), that flows around the basin. The initial, slow restratification resulted from the weak horizontal density gradients created by the widespread 2015 atmospheric heat loss. Faster restratification occurred once the IC recovered. This mechanism explains the delayed recovery of the Irminger Sea following a single extreme winter and has implications for the ventilation and overturning that occurs in the basin.

Plain Language Summary The Irminger Sea, between Greenland and Iceland, is known to be an important driver of variability in the global ocean circulation that regulates global climate. During the 2015 winter, the Irminger Sea experienced widespread cooling and buoyancy loss down to 1,000 m, resulting in deeper wintertime mixing than had been observed in the region for many years. This low buoyancy state and deep wintertime mixing persisted from 2015 to 2018, despite a return to average atmospheric wintertime conditions. Here we study how processes that typically provide summertime buoyancy gain to balance wintertime buoyancy loss contribute to the multi-year recovery of the region. We characterize the recovery of the interior of the Irminger Sea as having two stages: initially slow recovery, followed by more rapid recovery. Our findings are consistent with earlier studies stating that the main source of buoyancy to the interior is eddies shed from the current flowing around the Irminger Sea. This study shows that the deep mixing that is important for global circulation and climate is influenced by changes in the current around the basin.

1. Introduction

The Irminger Sea plays a key role in climate due to the unique local ocean-atmosphere conditions that allow for deep convection and water mass transformation, feeding the Atlantic Meridional Overturning Circulation (AMOC) and ventilating the deep ocean (de Jong et al., 2012; Katsman et al., 2018; Le Bras et al., 2020; Pickart et al., 2003). The rate of intermediate water formation regulates AMOC strength and oxygen and carbon dioxide concentrations at intermediate depths (Palevsky & Nicholson, 2018; Petit et al., 2020). As such, variability in local stratification, which affects intermediate water formation, is of interest for understanding global climate (Chafik et al., 2022; Lozier et al., 2019; Pérez et al., 2013; Rhein et al., 2017; Takahashi et al., 2009; Tjiputra et al., 2018).

In 2015, strong winter atmospheric forcing resulted in anomalously deep mixed layer depths (>1,400 m) and the expansion of the intermediate water layer and thinning of the light water layer within the Irminger Sea (de Jong & de Steur, 2016; de Jong et al., 2018). While 2015 was the first year of deep convection in the region since the early 1990s (Våge et al., 2011), deep convection persisted to depths of >1,300 m through 2018, despite a return to normal atmospheric forcing (Fox et al., 2022; Zunino et al., 2020). The persistence of relatively deep convection in the Irminger Sea, even under moderate atmospheric forcing, is indicative of a slow recovery of the Irminger Sea to pre-2015 conditions. Because of this slow recovery, the injection of oxygen and carbon to intermediate depths likely persisted with potential implications for carbon sequestration (Fröb et al., 2016).

Writing – original draft: Monica Nelson
Writing – review & editing: Monica Nelson, Fiamma Straneo, Sarah G. Purkey, Marieke Femke de Jong

The recovery of the Irminger Sea is dictated by the restratification processes which converge warm, buoyant water on the interior, thickening the light water layer. Models and observations show that restratifying waters are advected from the boundary currents by eddies (Fan et al., 2013; Gelderloos et al., 2011; Katsman et al., 2004; Spall, 2004; Sterl & de Jong, 2022; Straneo, 2006a, 2006b). In the Labrador Sea, these eddies are known to be produced by baroclinic instabilities in the boundary current (de Jong et al., 2016; Spall, 2004; Straneo, 2006a; Visbeck et al., 1996). In the Irminger Sea, Sterl and de Jong (2022) show that interannual variations in the seasonal restratification are strongly correlated with eddy kinetic energy (EKE) but do not explain what drives EKE variability.

The anomalous densification of the Irminger Sea in 2015 provided a unique opportunity to study restratification processes in the basin. We use repeat hydrography, an Argo product, and EKE from a satellite product to observe changes in both the Irminger interior and Irminger Current (IC) and investigate the dynamics that converge buoyancy on the interior. We show that while the 2015 wintertime buoyancy loss affected both the interior and the IC, the IC regains buoyancy much more quickly than the interior. The slow timescale for the recovery of the interior is primarily set by the time needed for the development of a large horizontal buoyancy gradient between the interior and IC. We show that the multi-year recovery processes and timescales in the Irminger Sea are a consistent extension of the seasonal restratification dynamics that have been described in the Labrador Sea.

2. Data

Conductivity, Temperature, Depth profiles collected along repeat occupations of the AR07-E hydrographic section (Figure 1a, bold black line) are used to observe full-depth changes in basin-wide potential density structure over the study period (Figures 1b–1d). Eight occupations between 2010 and 2022 are used: biennial occupations between 2010 and 2018 by the Observatoire de la variabilité interannuelle et décennale en Atlantique Nord (OVIDE) project, and occupations in 2015, 2020, and 2022 by the Overturning in the Subpolar North Atlantic Program (OSNAP). All sections were conducted in either June or July, except the 2014 section which was conducted in May and the 2022 section which was conducted in August. No additional data quality control was carried out.

Temperature and salinity from the Roemmich and Gilson Argo gridded climatology and anomalies (RG product) from January 2011 to December 2022 within the Irminger Sea are used to estimate the temporal variability in horizontal and vertical density structure. The RG product uses only adjusted, delay mode quality controlled Argo profiles with additional screening to exclude any floats with salinity drift to give monthly objective maps of temperature and salinity on 58 pressure levels between 0 and 2,000 dbar on a 1° × 1° grid (Roemmich & Gilson, 2009).

Eddy activity is quantified using the AVISO EKE product (AVISO+Altimetry, 2021). The product is derived from satellite altimetry and has a spatial resolution of 1/4° on a monthly time-step.

3. Methods

The study period, January 2011 to December 2022, is split into three periods: pre-strong convection (January 2011 to March 2015), during strong convection (April 2015 to March 2018), and post-strong convection (April 2018 to December 2022). Temperature and salinity profiles from each AR07-E occupation are interpolated onto a regular 2D grid and averaged over each period to create composite summertime potential density sections across the Irminger Sea (Figures 1b–1d).

Within the Irminger Sea the study focuses on two regions: the interior and the IC on the eastern boundary (Figure 1a, red and magenta crosses respectively). While exchange of waters is also known to occur on the western boundary, through eddies (Fan et al., 2013; Le Bras et al., 2020) and slantwise convection (Le Bras et al., 2022), the western boundary is notably less buoyant than the eastern boundary (Figure 1) (Våge et al., 2011) with less available potential energy for the development of baroclinic instabilities (Pedlosky, 1979). As such, it is expected that exchange with the eastern boundary dominates the convergence of buoyant water on the interior. This is consistent with idealized and observational studies in both the Labrador and Irminger Seas (Spall, 2004; Sterl & de Jong, 2022; Straneo, 2006b; Våge et al., 2011); with Fan et al. (2013) showing that the most buoyant eddies found in the Irminger interior are from the eastern boundary. Thus, we create spatially-averaged time-series of

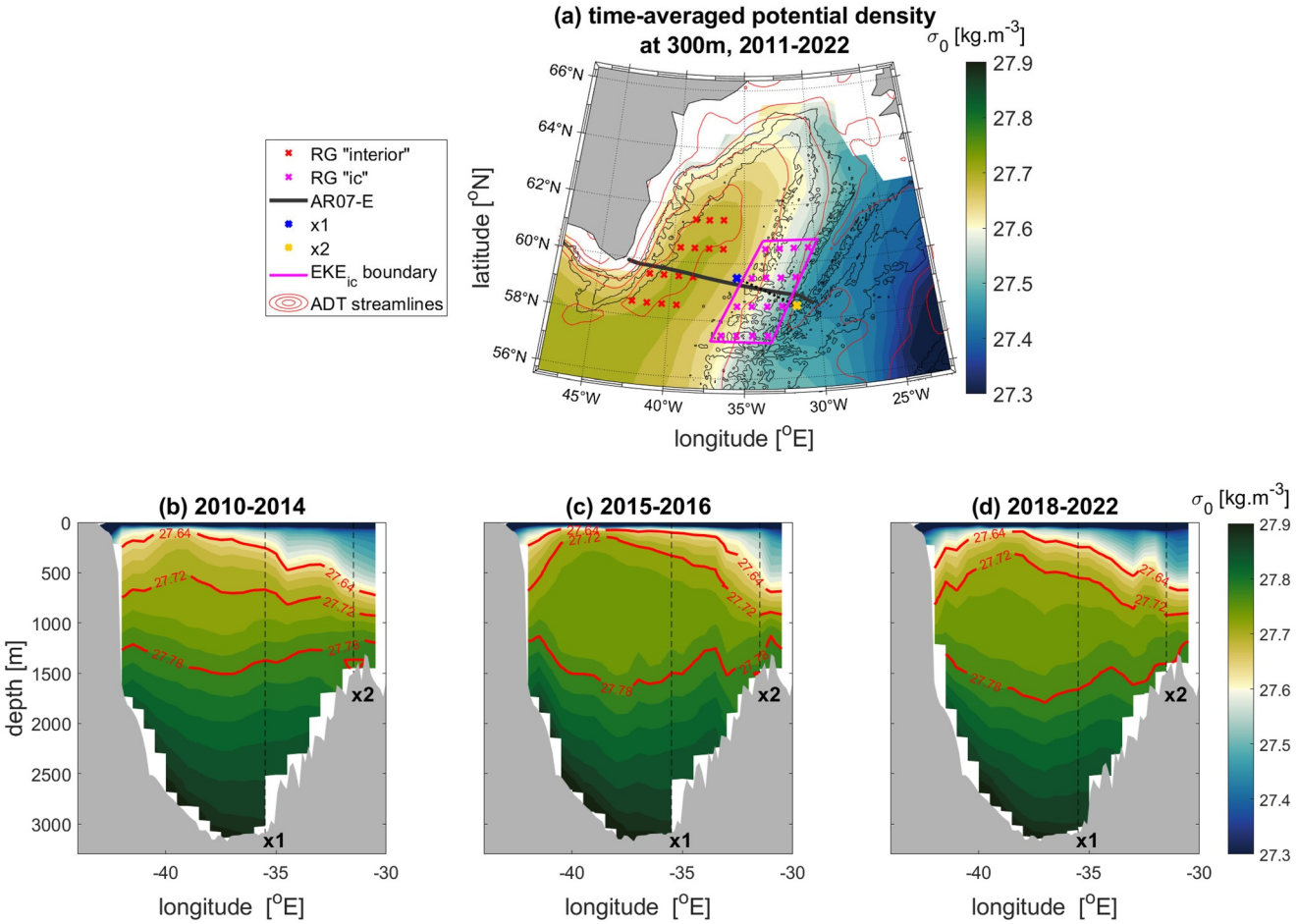

Figure 1. (a) Potential density at 300 m in the Irminger Sea with 1,500, 2,000, and 2,500 m isobaths (thin black lines) and Absolute Dynamic Topography streamlines (red) overlain to illustrate the mean circulation. Locations of data used in this paper are also shown: RG grid-points used in the interior area average (red crosses); RG grid-points used in the Irminger Current (IC) area average (magenta crosses); AR07-E hydrographic section (bold black line); x1 (blue cross) and x2 (yellow cross) between which ΔB_x is calculated; and the region over which the area-averaged EKE_{ic} is calculated (magenta box). Mean potential density AR07-E hydrographic sections across the Irminger Sea averaged over the (b) pre-strong convection period (2010, 2012, 2014); (c) during strong convection period (2015 and 2016); and (d) post-strong convection period (2018, 2020, and 2022), with the 27.64, 27.72, and 27.78 kg.m^{-3} isopycnals (red) and the locations of x1 and x2 for the ΔB_x calculation (black dashed) overlain.

potential density for only the interior and IC on the eastern boundary using the RG product (Figures 2a and 2b). Potential density referenced to the surface is calculated at each grid-point then an area-averaged potential density profile is calculated for the interior and IC.

Similarly, a time-series of the depth-integrated buoyancy content in the 100–1,000 m layer is calculated for the interior and IC using the RG product (Figure 2c). First, area-averaged in situ density profiles are calculated for the interior and the IC as above. Second, the buoyancy content within the interior, B_{int}, and IC, B_{ic}, is calculated as

$$B = -g \int_{-1{,}000}^{-100} \left(\frac{\rho(z) - \rho_0}{\rho_0} \right) dz \tag{1}$$

where $\rho(z)$ is the average in situ density profile in each region, ρ_0 is defined to be 1,037 kg m^{-3} representing the densest water in the upper 2,000 m, and g is the gravitational constant.

The rates of recovery of the interior and IC are defined as the rate at which buoyancy is gained in each region. The rates are estimated by using a Least Squares fit of a linear trend with a seasonal cycle to the time-series of B_{int} and B_{ic}:

$$\hat{B} = a + mt + c\ \sin(\omega t) + d\ \cos(\omega t) \tag{2}$$

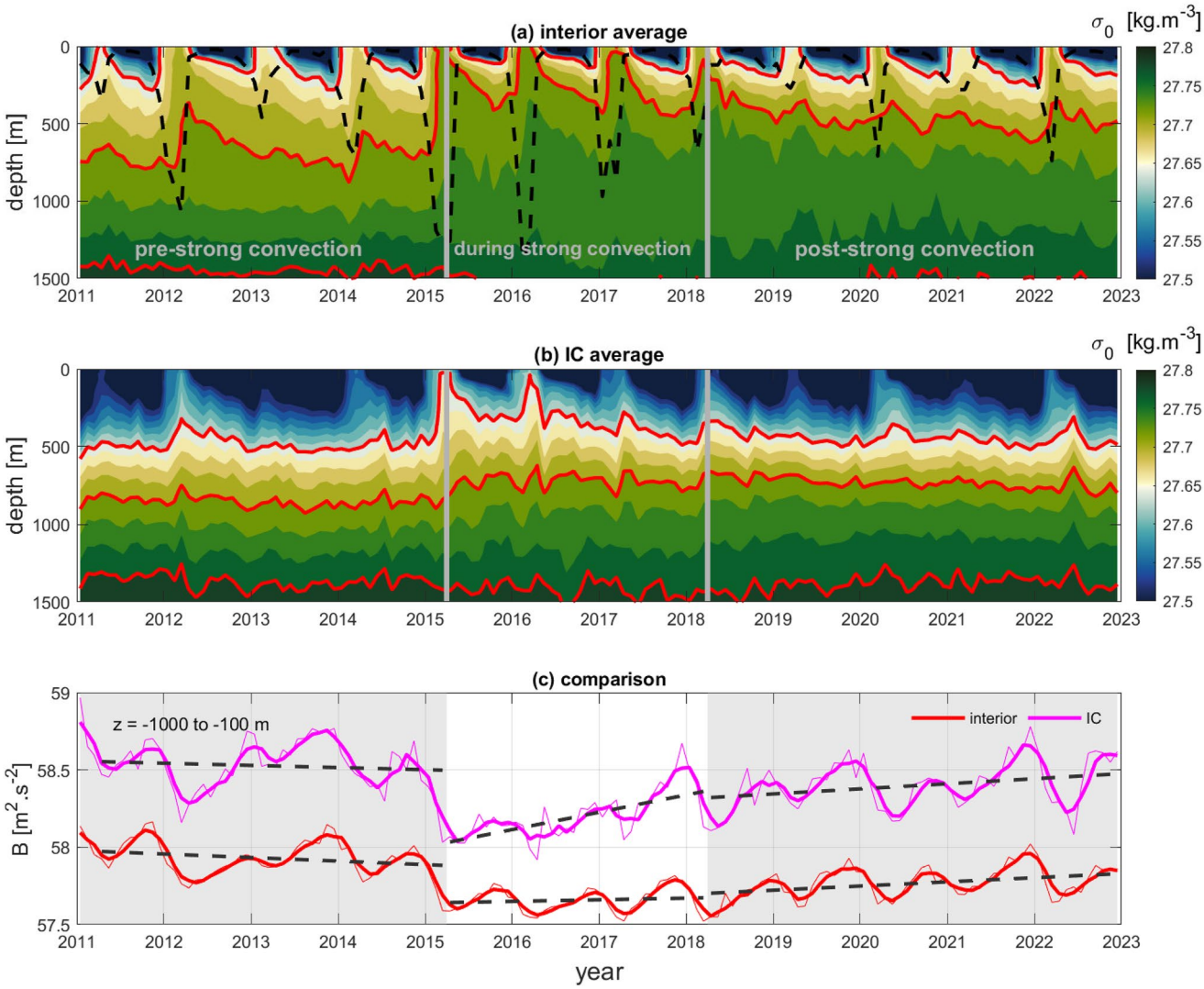

Figure 2. Time-series of the area-averaged potential density in the (a) interior and (b) Irminger Current (IC) (see Figure 1a for locations), in the upper 1,500 m with the 27.64, 27.72, and 27.78 kg.m^{-3} isopycnals overlain (red). The mixed layer depth (black dashed) is shown in (a). (c) Depth-integrated buoyancy content over the 100–1,000 m layer for the interior (red) and IC (pink); thin lines show the raw monthly time-series, thick lines show the smoothed time-series after applying a 4-month moving mean. Thick black dashed lines show linear trend from Least Squares fit for each period.

where coefficients, a, m, c, and d are optimized for the fit. m is the linear trend, c and d determine the amplitude of the seasonal cycle, and ω is the period of the seasonal cycle (Wunsch, 1996).

The seasonal restratification of the interior is quantified by the buoyancy gained in the interior over the restratification period. The restratification period is defined as the time from minimum B_{int} to maximum B_{int} each year such that the buoyancy gain during restratification is $B_{int}^{gain} = \max(B_{int}) - \min(B_{int})$ (Figures 3b and 3c).

Lastly, the horizontal density gradient across the IC is approximated by differencing the buoyancy content between an inner point (x1) and an outer point (x2) of the IC (Figure 1a) using Equation 1 at each time step, $\Delta B_x = B_{x2} - B_{x1}$ (Figure 3a). Following Spall (2004) and Straneo (2006a), we square ΔB_x at the start of the restratification period each year (Figure 3b). ΔB_x^2 is used as the horizontal buoyancy difference sets both the number of eddies and the additional buoyancy content the eddies can transport to the interior (Spall, 2004). Additionally, EKE is quantified by spatially averaging all AVISO grid-points in the IC region (EKE_{ic}, Figure 1a) and taking the time-mean over the restratification period each year (EKE_R, Figure 3c). We then calculate linear correlations between ΔB_x^2 and B_{int}^{gain} (r_{Bx}) and EKE_R and B_{int}^{gain} (r_{eke}), as in Straneo (2006a) and Sterl and de Jong (2022) respectively.

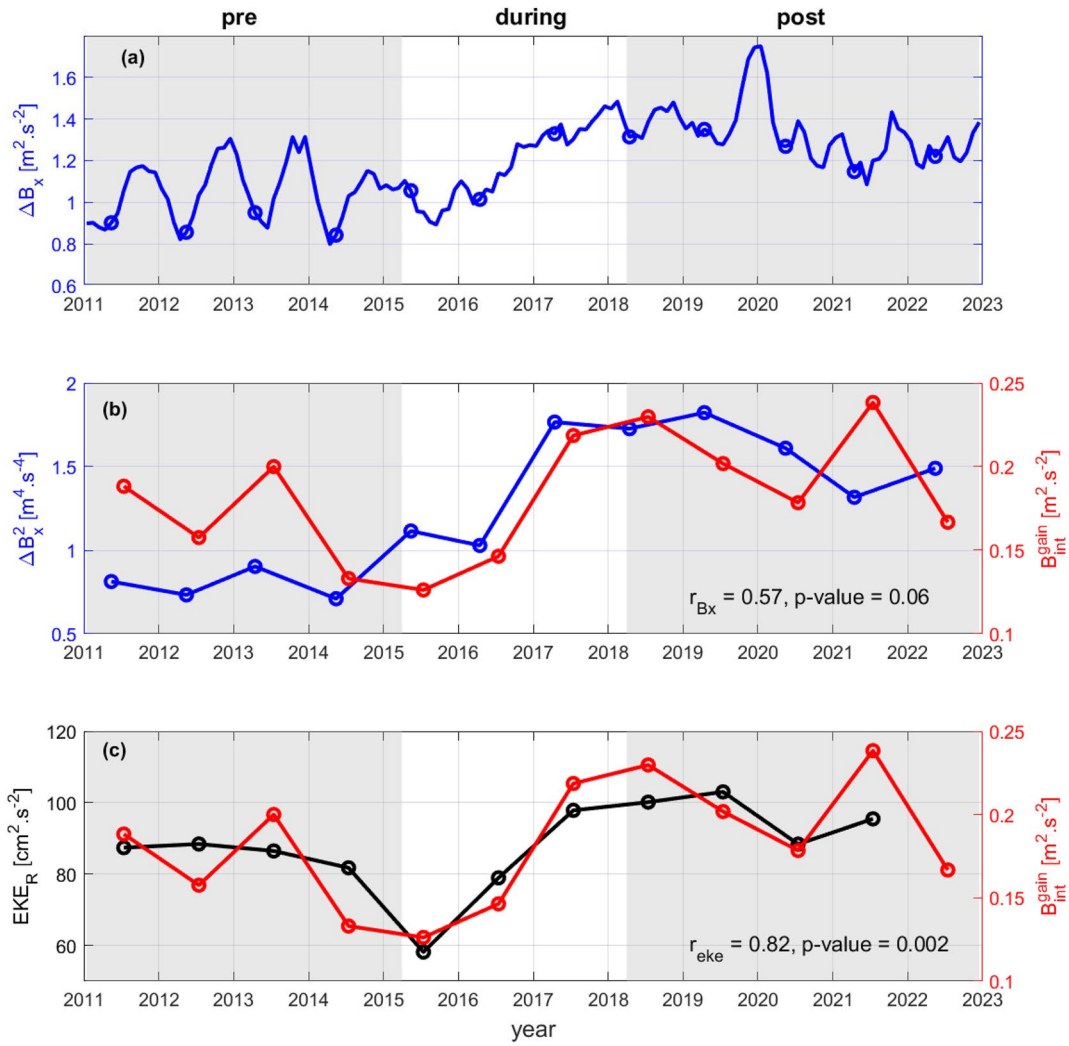

Figure 3. (a) Monthly time-series of the horizontal difference in buoyancy content (integrated over the 100–1,000 m layer) across the Irminger Current (IC), from x1 to x2 (see Figure 1a), circles show the ΔB_x value at the start of the restratification period. (b) Comparison of the interannual variability in the square of the horizontal difference in buoyancy content over the IC at the start of the restratification period, ΔB_x^2 (blue) and the buoyancy content gain in the interior over the restratification period in the 100–1,000 m layer, B_{int}^{gain} (red). (c) Comparison of the interannual variability in the average eddy kinetic energy (EKE) in the IC region during the restratification period, EKE_R (black) and B_{int}^{gain} (red).

See Supporting Information S1 for a more detailed description of the methods.

4. Results

The anomalous water mass transformation that occurred in 2015 notably changed the density structure of the whole Irminger Sea (Figures 1b–1d). Following the 2014/2015 winter there is thinning of the light water layer (27.64–27.72 kg.m^{-3}) and a thickening of intermediate water layer (27.72–27.78 kg.m^{-3}) across the Irminger interior, consistent with de Jong and de Steur (2016) and de Jong et al. (2018). Thickening of the intermediate water layer is also seen on both the eastern (between x1 and x2) and western (between −44°E and −42°E) boundaries, resulting in a steepening of the horizontal density gradients (Figure 1c). Between 1,000 and 1,500 m, in the interior isopycnals deepen due to the convergence of anomalously fresh intermediate water recirculating from the Labrador Sea (Fox et al., 2022; Zunino et al., 2020); whereas there is little change at depth on the boundaries. In the post-strong convection period the density structure is returning to the pre-strong convection state, with a deepening of the 27.64 and 27.72 kg.m^{-3} isopycnals in the interior and a flattening of the isopycnal slope across the boundaries (Figure 1d).

Table 1
Rates of Recovery in the Irminger Interior Compared to Those in the Irminger Current for the During-Strong Convection Period (April 2015 to March 2018) and the Post-Strong Convection Period (April 2018 to December 2022)

	Recovery rate 2015–2018 ($\times 10^{-3}$ m^2 s^{-2} month^{-1})	Recovery rate 2018–2022 ($\times 10^{-3}$ m^2 s^{-2} month^{-1})	Percent recovered by March 2018 (3 years) (%)	Percent recovered by December 2022 (8 years) (%)
Irminger interior	0.9 ± 0.5	2.7 ± 0.6	12	79
Irminger Current	9.3 ± 1.0	2.2 ± 0.3	70	94

As discussed in Section 3 we now focus on the interior and the IC on the eastern boundary and find that the two regions recover from the density anomaly differently (Figure 2, Table 1). In the interior, the density anomaly persists from 2015 through 2018, after which isopycnals above 1,000 m begin to deepen (Figure 2a). This is reflected in the slow rate of buoyancy gain in the interior in the first 3 years after 2015, followed by more rapid gain in the subsequent 5 years (Figure 2c, red). In contrast, in the IC, the density anomaly is quickly exported, with the 27.64 kg.m^{-3} isopycnal deepening rapidly in 2015 and 2016, then stabilizing after 2018 (Figure 2b). This is seen in the rapid gain of buoyancy in the IC in the first 3 years after 2015, followed by slower gain in the subsequent 5 years (Figure 2c, pink). Estimates of the rates of recovery for the interior and IC are shown in Table 1.

The difference in the evolution of the buoyancy content in the interior and the IC results in a change in the horizontal buoyancy gradient across the IC, ΔB_x (Figure 3a). Before the onset of strong convection ΔB_x oscillates around 1 m^2 s^{-2}. In 2015 there is little change in the mean of ΔB_x as both the buoyancy content on the inner and outer edge of the IC decrease similarly. However, from 2016 to 2018, there is a steady increase in ΔB_x due to the more rapid increase in buoyancy on the outer edge of the IC (at x2) than on the inner edge (at x1). In the years after 2018 ΔB_x appears to decrease slightly, consistent with eddy flux from the IC to the interior working to flatten the isopycnal gradient.

Lastly, the buoyancy gain during restratification is compared to the horizontal buoyancy gradient and the EKE. Changes in the horizontal buoyancy difference are correlated with changes in the buoyancy gain in the interior over the restratification period, with $r_{Bx} = 0.57$ ($p = 0.06$) (Figure 3b). The correlation between EKE and buoyancy gain is even higher, with $r_{eke} = 0.82$ ($p = 0.002$) (Figure 3c). While these correlations are calculated at zero lag, each data point is an average over the 8-month restratification period such that any lag on shorter timescales, for example, due to the duration of eddy advection, is lost. This high correlation at zero lag is consistent with Fan et al. (2013) who show that eddies with lifetimes of around 4 months travel from the IC to the interior. The improved correlation between EKE and buoyancy gain during restratification indicates that while baroclinic instabilities are likely a major source of buoyancy they are not the only eddy mechanism transporting buoyancy into the interior.

5. Discussion

These results show that restratification dynamics govern the differing rates of recovery of the interior and IC from an anomalously dense and weakly stratified state. Due to the widespread nature of the density anomaly (de Jong et al., 2020; Josey et al., 2019), the IC becomes noticeably denser in 2015 such that there is initially very little change in the horizontal buoyancy gradient between the interior and IC (Figures 3a and 3b). As the IC is a fast-flowing current (Våge et al., 2011), the anomalously cold waters are flushed from the region relatively rapidly and replenished by lighter, warmer waters from upstream. The recovery of the IC results in an increase in the horizontal buoyancy gradient between the interior and IC from 2016 to 2018, driving faster flow in the IC from 2018 to 2020 (Fried & Jong, 2022) coincident with a peak in the seasonal buoyancy gain in the interior. This is consistent with baroclinic instabilities resulting in an eddy flux of buoyancy into the interior, as proposed by de Jong et al. (2016), Spall (2004), and Straneo (2006a).

The recovery of each region can be roughly quantified by comparing the deficit in buoyancy content at a given time, relative to the buoyancy content in March 2015 and with the seasonal cycle removed, to the deficit in April 2015 (Table 1). While it is expected that the recovery of the interior will take longer than that of the IC given its isolated nature, the interior only recovers 12% of the lost buoyancy in the first 3 years—recovering far slower

than the typical restratification timescale of a single season (Straneo, 2006a). We propose this is due to buoyancy loss in the IC resulting in, initially, little change in the horizontal buoyancy gradient, limiting convergence of buoyancy by baroclinic instabilities and delaying the recovery. Notably, the 8 years it takes the interior to recover 79% of the buoyancy deficit is much longer than the single season the buoyancy was lost over and is similar to the 10 years that typically separate strong convective events in the Irminger and Labrador Seas (de Jong & de Steur, 2016; van Aken et al., 2011).

While many processes drive exchange between the boundary current and the interior, only a few processes converge buoyancy (i.e., light waters) into the interior. In addition to baroclinic instabilities, baroclinic Rossby waves and other eddy generating mechanisms (e.g., barotropic instabilities) on the eastern boundary may provide an additional buoyancy flux to the interior (Våge et al., 2011). These processes could explain the stronger correlation of buoyancy gain at the interior with EKE than with the horizontal buoyancy gradient. Additional processes may contribute to exchange of intermediate and dense water, such as export on the western boundary (Le Bras et al., 2020, 2022) and recirculation in the Irminger gyre (Våge et al., 2011). Here we assume that the effect of these processes on the rate of convergence of light water on the interior is small compared to the baroclinic instability process described above.

The delayed recovery of the interior has implications for wintertime convection. Zunino et al. (2020) found that deep convection was able to persist for 3 years following the strong winter of 2015 due to pre-conditioning of the water column. We posit that the pre-conditioning lasted multiple years due to the lack of increased seasonal eddy-flux of buoyancy from the IC. Additionally, Biló et al. (2022) show that a surface salinity anomaly propagated around the Irminger Sea during the late 2010s, suggesting that freshwater accumulation in the interior caused strong convection to cease after 2018. Our results suggest that the freshening of the boundary current may have contributed to the buoyancy gain in the IC that led to the recovery of the interior and ended pre-conditioning.

There are a couple limitations of the analysis presented here. First, the AVISO EKE product only resolves large eddies, with a resolution of ∼40 km (Chelton et al., 2011), so smaller-scale turbulence and mixing resulting in exchange between the IC and the interior are not captured here. Second, the parameterization developed by Spall (2004) to describe the eddy flux of buoyancy is based on a model of the Labrador basin, but the Irminger basin has notably different bathymetry: on its eastern boundary the Irminger Sea is bounded by the relatively shallowly sloping Reykjanes Ridge (in a large-scale sense when averaging over very rough small-scale bathymetry). The parameterization given by Spall (2004) is expected to hold when the bottom slope is less than 1.5 times the isopycnal slope, which is not the case at any point in the time-period studied here. However, the relatively high correlation between the buoyancy gain during restratification and the square of the horizontal buoyancy gradient suggests that the parameterization holds moderately well. Additionally, the steeper bottom slope on the western boundary still supports the assumption that the eastern boundary is the main source of waters that converge buoyancy to restratify the interior.

In addition to clarifying the restratification process, these results also have important implications for ocean biogeochemistry. Feucher et al. (2022) found that the main drivers of the oxygen variability in the region were changes in vertical mixing and horizontal advection, but do not specifically explore eddy-advection from the IC. Given that oxygen concentrations are known to be low over the Reykjanes Ridge (Petit et al., 2019) we suggest that changes in the eddy-flux of water from the IC may contribute to variability in oxygen concentrations in the interior, in addition to the delayed recovery allowing for reventilation of waters not yet exported from the interior (Feucher et al., 2022). Further work is needed to determine whether variability in eddy-flux from the IC significantly affects the oxygen budget of the Irminger interior.

6. Conclusion

The densification of the Irminger Sea in 2015 provided an opportunity to study the dynamics of the subsequent restratification and recovery. We find that the recovery of the Irminger interior was two-stage: an initial slow buoyancy gain while the IC recovered, which set up the necessary conditions to drive a more rapid second-stage recovery of the interior. The restratification of the subsurface water column is shown to be due to eddy-shedding from the IC along the Reykjanes Ridge, primarily as a result of baroclinic instabilities. This result is consistent with findings in the Labrador Sea (de Jong et al., 2016; Spall, 2004; Straneo, 2006a) and speculations about the Irminger Sea (Fan et al., 2013; Sterl & de Jong, 2022). The delayed recovery of the interior is a direct outcome of

the changing horizontal density gradient that drives growth of baroclinic instabilities. Because of the two-stage recovery, deep convection in the interior persisted for multiple years in a row, with implications for local biogeochemistry (Feucher et al., 2022). This work shows it is important to consider changes in the IC when considering drivers of variability in stratification, water mass transformation, ventilation and AMOC.

Data Availability Statement

The AR07-E hydrographic section data was gathered by the OVIDE program and the OSNAP program. The OVIDE sections are available at https://www.seanoe.org/data/00353/46448/ (Herle et al., 2022). The 2015 OSNAP section data is available at https://www.seanoe.org/data/00481/59302/ (de Jong & de Steur, 2019). The 2020 OSNAP data is available https://dataverse.nioz.nl/dataset.xhtml?persistentId=doi:10.25850/nioz/7b.b.1f (de Jong, 2023). The 2022 OSNAP section data is available at https://cchdo.ucsd.edu/cruise/33VB20220819 (Straneo, 2023).

The Roemmich and Gilson Argo data product is available at https://sio-argo.ucsd.edu/RG_Climatology.html (Roemmich & Gilson, n.d.). The Roemmich and Gilson data product is produced using data that were collected and made freely available by the International Argo Program and the national programs that contribute to it http://www.argo.ucsd.edu, http://argo.jcommops.org (Argo, 2024). The Argo Program is part of the Global Ocean Observing System.

The Eddy Kinetic Energy product is freely available through AVISO+. Those products were processed by SSALTO/DUACS and distributed by AVISO+ at https://www.aviso.altimetry.fr with support from CNES (AVISO+Altimetry, n.d.).

Acknowledgments
We gratefully acknowledge the U.S. National Science Foundation: this work was supported by Grants OCE-1756272 and OCE-1948482. S.G.P. was supported by NOAA Grant NA20OAR4320278. MF de Jong is financially supported by the Innovational Research Incentives Scheme of the Netherlands Organisation for Scientific Research (NWO) under Grant 016.Vidi.189.130. We thank all the field teams (scientists, technical staff and crew) that made the hydrographic data collection possible. We thank Tiago Biló for providing the streamlines for the average circulation in the Irminger Sea in from 2006 to 2020 (Figure 1a). We thank the reviewers for their rapid responses and comments which helped to improve the manuscript.

References

Argo. (2024). Argo float data and metadata from Global Data Assembly Centre (Argo GDAC). SEANOE. https://doi.org/10.17882/42182

AVISO+Altimetry. (n.d.). Monthly mean and climatology maps of sea level anomalies - EKE [Dataset]. AVISO+. Retrieved from https://tds.aviso.altimetry.fr/thredds/catalog/dataset-duacs-climatology-global/delayed-time/monthly_mean/catalog.html

AVISO+Altimetry. (2021). *SSALTO/DUACS user handbook: Eddy Kinetic Energy (EKE) monthly mean products*. CNES. Retrieved from https://www.aviso.altimetry.fr/fileadmin/documents/data/tools/monthly_mean_eke_hdbk.pdf (SALP-MU-P-EA-23506-CLS).

Biló, T. C., Straneo, F., Holte, J., & Le Bras, I. A.-A. (2022). Arrival of new great salinity anomaly weakens convection in the Irminger Sea. *Geophysical Research Letters*, *49*(11), e2022GL098857. https://doi.org/10.1029/2022GL098857

Chafik, L., Holliday, N. P., Bacon, S., & Rossby, T. (2022). Irminger Sea is the center of action for subpolar AMOC variability. *Geophysical Research Letters*, *49*(17), e2022GL099133. https://doi.org/10.1029/2022GL099133

Chelton, D. B., Schlax, M. G., & Samelson, R. M. (2011). Global observations of nonlinear mesoscale eddies. *Progress in Oceanography*, *91*(2), 167–216. https://doi.org/10.1016/j.pocean.2011.01.002

de Jong, M. F. (2023). Calibrated CTD data from OSNAP Pelagia cruise 64PE473 in July–Aug 2020 [Dataset]. NIOZ. https://doi.org/10.25850/nioz/7b.b.1f

de Jong, M. F., Bower, A. S., & Furey, H. H. (2016). Seasonal and interannual variations of Irminger ring formation and boundary–interior heat exchange in FLAME. *Journal of Physical Oceanography*, *46*(6), 1717–1734. https://doi.org/10.1175/JPO-D-15-0124.1

de Jong, M. F., & de Steur, L. (2016). Strong winter cooling over the Irminger Sea in winter 2014-2015, exceptional deep convection, and the emergence of anomalously low SST: Irminger Sea cooling and convection. *Geophysical Research Letters*, *43*(13), 7106–7113. https://doi.org/10.1002/2016GL069596

de Jong, M. F., & de Steur, L. (2019). Cruise 64PE400: Hydrographic survey of the Irminger Sea in July 2015 for the Overturning in the Subpolar North Atlantic Program (OSNAP) [Dataset]. SEANOE. https://doi.org/10.17882/59302

de Jong, M. F., de Steur, L., Fried, N., Bol, R., & Kritsotalakis, S. (2020). Year-round measurements of the Irminger current: Variability of a two-core current system observed in 2014–2016. *Journal of Geophysical Research: Oceans*, *125*(10), e2020JC016193. https://doi.org/10.1029/2020JC016193

de Jong, M. F., Oltmanns, M., Karstensen, J., & de Steur, L. (2018). Deep convection in the Irminger Sea observed with a dense mooring array. *Oceanography*, *31*(1), 50–59. https://doi.org/10.5670/oceanog.2018.109

de Jong, M. F., van Aken, H. M., Våge, K., & Pickart, R. S. (2012). Convective mixing in the central Irminger Sea: 2002–2010. *Deep Sea Research Part I: Oceanographic Research Papers*, *63*, 36–51. https://doi.org/10.1016/j.dsr.2012.01.003

Fan, X., Send, U., Testor, P., Karstensen, J., & Lherminier, P. (2013). Observations of Irminger Sea anticyclonic eddies. *Journal of Physical Oceanography*, *43*(4), 805–823. https://doi.org/10.1175/JPO-D-11-0155.1

Feucher, C., Portela, E., Kolodziejczyk, N., & Thierry, V. (2022). Subpolar gyre decadal variability explains the recent oxygenation in the Irminger Sea. *Communications Earth & Environment*, *3*(1), 1–9. https://doi.org/10.1038/s43247-022-00570-y

Fox, A. D., Handmann, P., Schmidt, C., Fraser, N., Rühs, S., Sanchez-Franks, A., et al. (2022). Exceptional freshening and cooling in the eastern subpolar North Atlantic caused by reduced Labrador Sea surface heat loss. *Ocean Science*, *18*(5), 1507–1533. https://doi.org/10.5194/os-18-1507-2022

Fried, N., & Jong, M. F. D. (2022). The role of the Irminger Current in the Irminger Sea northward transport variability. *Journal of Geophysical Research: Oceans*, *127*(3), e2021JC018188. https://doi.org/10.1029/2021JC018188

Fröb, F., Olsen, A., Våge, K., Moore, G. W. K., Yashayaev, I., Jeansson, E., & Rajasakaren, B. (2016). Irminger Sea deep convection injects oxygen and anthropogenic carbon to the ocean interior. *Nature Communications*, *7*(1), 1–8. https://doi.org/10.1038/ncomms13244

Gelderloos, R., Katsman, C. A., & Drijfhout, S. S. (2011). Assessing the roles of three eddy types in restratifying the Labrador Sea after deep convection. *Journal of Physical Oceanography*, *41*(11), 2102–2119. https://doi.org/10.1175/JPO-D-11-054.1

Herle, M., Pascale, L., & Pérez, F. F. (2022). The Greenland-Portugal Go-Ship A25 OVIDE CTDO2 hydrographic data [Dataset]. SEANOE. https://doi.org/10.17882/46448

Josey, S. A., de Jong, M. F., Oltmanns, M., Moore, G. K., & Weller, R. A. (2019). Extreme variability in Irminger Sea winter heat loss revealed by ocean observatories initiative mooring and the ERA5 reanalysis. *Geophysical Research Letters*, *46*(1), 293–302. https://doi.org/10.1029/2018GL080956

Katsman, C. A., Drijfhout, S. S., Dijkstra, H. A., & Spall, M. A. (2018). Sinking of dense North Atlantic waters in a global ocean model: Location and controls. *Journal of Geophysical Research: Oceans*, *123*(5), 3563–3576. https://doi.org/10.1029/2017JC013329

Katsman, C. A., Spall, M. A., & Pickart, R. S. (2004). Boundary current eddies and their role in the restratification of the Labrador Sea. *Journal of Physical Oceanography*, *34*(9), 1967–1983. https://doi.org/10.1175/1520-0485(2004)034⟨1967:BCEATR⟩2.0.CO;2

Le Bras, I. A.-A., Callies, J., Straneo, F., Biló, T. C., Holte, J., & Johnson, H. L. (2022). Slantwise convection in the Irminger Sea. *Journal of Geophysical Research: Oceans*, *127*(10), e2022JC019071. https://doi.org/10.1029/2022JC019071

Le Bras, I. A.-A., Straneo, F., Holte, J., de Jong, M. F., & Holliday, N. P. (2020). Rapid export of waters formed by convection near the Irminger Sea's western boundary. *Geophysical Research Letters*, *47*(3), e2019GL085989. https://doi.org/10.1029/2019GL085989

Lozier, M. S., Li, F., Bacon, S., Bahr, F., Bower, A. S., Cunningham, S. A., et al. (2019). A sea change in our view of overturning in the subpolar North Atlantic. *Science*, *363*(6426), 516–521. https://doi.org/10.1126/science.aau6592

Palevsky, H., & Nicholson, D. (2018). The North Atlantic biological pump: Insights from the ocean observatories initiative Irminger Sea array. *Oceanography*, *31*(1), 42–49. https://doi.org/10.5670/oceanog.2018.108

Pedlosky, J. (1979). *Geophysical fluid dynamics* (2nd ed.). Springer-Verlag.

Pérez, F. F., Mercier, H., Vázquez-Rodríguez, M., Lherminier, P., Velo, A., Pardo, P. C., et al. (2013). Atlantic Ocean CO_2 uptake reduced by weakening of the meridional overturning circulation. *Nature Geoscience*, *6*(2), 146–152. https://doi.org/10.1038/ngeo1680

Petit, T., Lozier, M. S., Josey, S. A., & Cunningham, S. A. (2020). Atlantic deep water formation occurs primarily in the Iceland Basin and Irminger Sea by local buoyancy forcing. *Geophysical Research Letters*, *47*(22), e2020GL091028. https://doi.org/10.1029/2020GL091028

Petit, T., Mercier, H., & Thierry, V. (2019). New insight into the formation and evolution of the East Reykjanes Ridge Current and Irminger Current. *Journal of Geophysical Research: Oceans*, *124*(12), 9171–9189. https://doi.org/10.1029/2019JC015546

Pickart, R. S., Spall, M. A., Ribergaard, M. H., Moore, G. W. K., & Milliff, R. F. (2003). Deep convection in the Irminger Sea forced by the Greenland tip jet. *Nature*, *424*(6945), 152–156. https://doi.org/10.1038/nature01729

Rhein, M., Steinfeldt, R., Kieke, D., Stendardo, I., & Yashayaev, I. (2017). Ventilation variability of Labrador Sea water and its impact on oxygen and anthropogenic carbon: A review. *Philosophical Transactions of the Royal Society A: Mathematical, Physical and Engineering Sciences*, *375*(2102), 20160321. https://doi.org/10.1098/rsta.2016.0321

Roemmich, D., & Gilson, J. (n.d.). Roemmich-Gilson Argo climatology [Dataset]. Retrieved from https://sio-argo.ucsd.edu/RG_Climatology.html

Roemmich, D., & Gilson, J. (2009). The 2004–2008 mean and annual cycle of temperature, salinity, and steric height in the global ocean from the Argo Program. *Progress in Oceanography*, *82*(2), 81–100. https://doi.org/10.1016/j.pocean.2009.03.004

Spall, M. A. (2004). Boundary currents and watermass transformation in marginal seas. *Journal of Physical Oceanography*, *34*(5), 1197–1213. https://doi.org/10.1175/1520-0485(2004)034⟨1197:BCAWTI⟩2.0.CO;2

Sterl, M. F., & de Jong, M. F. (2022). Restratification structure and processes in the Irminger Sea. *Journal of Geophysical Research: Oceans*, *127*(12), e2022JC019126. https://doi.org/10.1029/2022JC019126

Straneo, F. (2006a). Heat and freshwater transport through the central Labrador Sea. *Journal of Physical Oceanography*, *36*(4), 606–628. https://doi.org/10.1175/JPO2875.1

Straneo, F. (2006b). On the connection between dense water formation, overturning, and poleward heat transport in a convective basin*. *Journal of Physical Oceanography*, *36*(9), 1822–1840. https://doi.org/10.1175/JPO2932.1

Straneo, F. (2023). CTD data from 33VB20220819 [Dataset]. Retrieved from CCHDO https://cchdo.ucsd.edu/cruise/33VB20220819

Takahashi, T., Sutherland, S. C., Wanninkhof, R., Sweeney, C., Feely, R. A., Chipman, D. W., et al. (2009). Climatological mean and decadal change in surface ocean pCO_2, and net sea–air CO_2 flux over the global oceans. *Deep Sea Research Part II: Topical Studies in Oceanography*, *56*(8–10), 554–577. https://doi.org/10.1016/j.dsr2.2008.12.009

Tjiputra, J. F., Goris, N., Lauvset, S. K., Heinze, C., Olsen, A., Schwinger, J., & Steinfeldt, R. (2018). Mechanisms and early detections of multidecadal oxygen changes in the interior subpolar North Atlantic. *Geophysical Research Letters*, *45*(9), 4218–4229. https://doi.org/10.1029/2018GL077096

Våge, K., Pickart, R. S., Sarafanov, A., Knutsen, y., Mercier, H., Lherminier, P., et al. (2011). The Irminger Gyre: Circulation, convection, and interannual variability. *Deep Sea Research Part I: Oceanographic Research Papers*, *58*(5), 590–614. https://doi.org/10.1016/j.dsr.2011.03.001

van Aken, H. M., de Jong, M. F., & Yashayaev, I. (2011). Decadal and multi-decadal variability of Labrador Sea Water in the north-western North Atlantic Ocean derived from tracer distributions: Heat budget, ventilation, and advection. *Deep Sea Research Part I: Oceanographic Research Papers*, *58*(5), 505–523. https://doi.org/10.1016/j.dsr.2011.02.008

Visbeck, M., Marshall, J., & Jones, H. (1996). Dynamics of isolated convective regions in the ocean. *Journal of Physical Oceanography*, *26*(9), 1721–1734. https://doi.org/10.1175/1520-0485(1996)026⟨1721:DOICRI⟩2.0.CO;2

Wunsch, C. (1996). Basic machinery. In *The ocean circulation inverse problem* (pp. 92–211). Cambridge University Press. https://doi.org/10.1017/CBO9780511629570.005

Zunino, P., Mercier, H., & Thierry, V. (2020). Why did deep convection persist over four consecutive winters (2015–2018) southeast of Cape Farewell? *Ocean Science*, *16*(1), 99–113. https://doi.org/10.5194/os-16-99-2020

References From the Supporting Information

Frajka-Williams, E., Rhines, P. B., & Eriksen, C. C. (2014). Horizontal stratification during deep convection in the Labrador Sea. *Journal of Physical Oceanography*, *44*(1), 220–228. https://doi.org/10.1175/JPO-D-13-069.1

Volkov, D. L. (2005). Interannual variability of the altimetry-derived eddy field and surface circulation in the extratropical North Atlantic Ocean in 1993–2001. *Journal of Physical Oceanography*, *35*(4), 405–426. https://doi.org/10.1175/JPO2683.1